RERTR 2015 – 36TH INTERNATIONAL MEETING ON
REDUCED ENRICHMENT FOR RESEARCH AND TEST REACTORS

OCTOBER 11-14, 2015
THE PLAZA HOTEL
SEOUL, SOUTH KOREA

Grain Growth and Bubble Evolution in U-Mo Alloy by Multiscale Simulations

Zhi-Gang Mei, Linyun Liang, Yeon Soo Kim, Tom Wiencek, Gerard Hofman, Mihai Anitescu, Abdellatif M. Yacout
Argonne National Laboratory, 9700 South Cass Avenue, Argonne, IL 60439 – USA

ABSTRACT

Increased grain size in U-Mo dispersion fuel is believed to affect the fuel swelling at high fission density. In this work, a multiscale simulation approach combining first-principles calculation and phase-field modeling is used to investigate the grain growth behavior in U-Mo alloys. The material properties of U-Mo alloys predicted by first-principles calculations are incorporated into the mesoscale phase-field models to study the effect of annealing temperature, annealing time and the initial grain structures of fuel particles on the grain growth. The grain growth rate is evaluated and compared with experiment. Meanwhile, the gas bubble evolution kinetics in irradiated U-Mo alloy fuels is investigated to understand its effect on fuel swelling. We systematically examine the effect of Xe, vacancy, and SIA concentration, fission defect generation, and elastic interaction on the growth kinetics of gas bubble. The bubble size distribution and swelling of U-Mo are simulated and compared to experimental measurements.

1. Introduction details

U-Mo alloy is one of the most promising fuels for the future high performance research and test reactors due to its high uranium loading and stable irradiation behavior. At low burnups, the fission gas bubbles induced swelling of U-Mo fuel shows a linear dependence of fission density. Due to the high burnups pursued for U-Mo fuel, abnormal fuel swelling was observed at high burnups, which is believed to be closely related to a phenomenon called recrystallization. It was found that recrystallization starts at existing grain boundaries. Therefore, increasing the grain size and reducing the grain boundary area by heat treatment may effectively reduce swelling and increase the fuel performance. However, there are very few studies of grain growth of U-Mo alloy by heat treatment such as annealing. The purpose of this work is to investigate the grain growth of U-7Mo alloy using a combined first-principles and phase field method. Furthermore, the fission gas bubble evolution and resultant swelling in U-7Mo were studied by phase field models using realistic material properties predicted by first-principles calculations.

2. Computational methodology

2.1 First-principles calculations

To perform density functional theory (DFT) based first-principles calculations, we use the projector augmented wave method (PAW) [1] as implemented in the Vienna *ab initio* simulation package (VASP) [2, 3]. The exchange-correlation functional was described by the generalized gradient approximation (GGA) parameterized by Perdew Burke and Ernzerhof [4]. The $6s^2 6p^6 5f^2 7s^2$ and $4s^2 4p^6 4d^5 s^1$ electrons were treated as valence electrons for U and Mo, respectively. The atomic structures of U-Mo alloys were modeled by the SQS method using the Alloy Theoretic Automated Toolkit (ATAT) code [5, 6]. The standard method was used to construct the coincidence site lattice grain boundaries. The atomic structures for the STGBs were generated by GBstudio [7]. More details about the setup of DFT calculations can be found elsewhere [8].

2.2 Phase field models

2.2.1. Grain growth

Phase field variables $\eta_i(r)$ are chosen to distinguish the different orientations of grains. The total free energy of the interested system can be represented in a Ginsburg-Landau form as [9, 10]

$$F = \int \left[f_0(\eta_1, \eta_2, \dots, \eta_q) + \frac{1}{2}\kappa \sum_i \nabla^2 \eta_i(r) \right] d^3 r, \quad (1)$$

where f_0 is the local free energy density of the system, the second term is the gradient energy term and κ is its gradient coefficient [11].

The spatial and temporal evolutions of grain parameters follow the Allen-Cahn equation [12],

$$\frac{\partial \eta_i}{\partial t} = -L \frac{\delta F}{\delta \eta_i}, \; i = 1,2, \dots, q. \quad (2)$$

where L is the kinetic coefficient of grain boundary movement.

The temperature effect can be considered in the kinetic coefficient L according to the Arrhenius formula as [13]

$$L = L_0 e^{-\frac{Q}{k_B T}}, \quad (3)$$

where L_0 is a constant, k_B the Boltzmann's constant, T temperature, and Q the activation energy of grain boundary.

In order to quantitatively simulate the U-Mo materials based on the above model, the grain boundary energy, grain boundary mobility, and activation energy have to be determined by atomic calculations or experiments. In this work, the grain boundary energy will be calculated by using DFT. Based on this value, the expansion coefficients of chemical free energy and the gradient coefficient can be determined [14]. Due to the difficulty of calculating the grain boundary mobility, it will be calibrated by the experimental measurement of grain size at different time. The activation energy of the GB diffusion measured for Mo [15], i.e., 2.73 eV, is adopted in this work. We believe this value should be close to that for U-7Mo alloy, since Mo is the element with much slower diffusivity in U-Mo alloys [16].

The phase field model was implemented in a simulation code and the semi-implicit FFTW numerical method was employed to solve the Allen-Cahn equations [17]. Periodic boundary conditions were imposed on the simulation domain. The time step for the evolution is t = 0.8, and the spacing $\Delta x = \Delta y = 1.0$ μm. A model size of 200 μm×200 μm and the U-Mo plate size of 180 μm are used in the simulations.

2.2.2 Gas bubble evolution

To consider the Xe gas bubble evolution kinetics in the U-7Mo matrix under the irradiation condition, three parameters including the compositions $c_X(r,t)$ of Xe atom, $c_V(r,t)$ of vacancy, $c_I(r,t)$ of self-interstitial atom, which represent atoms or mole fractions at position r and time t, are chosen as composition fields. The phase parameter $\eta(r,t)$ is chosen to represent the gas bubble phase with $\eta = 1$ and the matrix with $\eta = 0$. The total energy of the system can be constructed as [18-20]

$$F(c_X, c_V, c_I, \eta, \varepsilon_{ij}) = \int \left[f_{chem}(c_X, c_V, c_I, \eta, T) + \frac{\kappa_X}{2}|\nabla c_X|^2 + \frac{\kappa_V}{2}|\nabla c_V|^2 + \frac{\kappa_I}{2}|\nabla c_I|^2 + \frac{\kappa_\eta}{2}|\nabla \eta|^2 + f_{elas}(c_X, \eta, \varepsilon_{ij}) \right] dV \quad , \quad (4)$$

where f_{chem} is the chemical free energy density describing the composition and volume fraction of the equilibrium phases, κ_X, κ_V, κ_I and κ_η are the gradient energy coefficients for Xe, vacancy, and self-interstitial atom (SIA) concentrations as well as the phase parameter, respectively, $f_{elas}(c_X, c_V, c_I, \varepsilon_{ij})$ is the elastic energy density. Detail expressions of the chemical free energy and elastic energy can be found in somewhere else [21].

The spatial and temporal evolutions of phase parameter and the Xe, vacancy and SIA compositions are controlled by the following equations as [18]

$$\frac{\partial \eta}{\partial t} = -L\frac{\delta F}{\delta \eta} + \dot{\xi}_\eta \quad (5a)$$

$$\frac{\partial c_X}{\partial t} = \nabla\left(M_X \nabla \frac{\delta F}{\delta c_X}\right) + \dot{\xi}_X + \dot{P}_X \quad (5b)$$

$$\frac{\partial c_V}{\partial t} = \nabla\left(M_V \nabla \frac{\delta F}{\delta c_V}\right) + \dot{\xi}_V + \dot{P}_V - \dot{R}_{VI} - \dot{S}_V \quad (5c)$$

$$\frac{\partial c_I}{\partial t} = \nabla\left(M_I \nabla \frac{\delta F}{\delta c_I}\right) + \dot{\xi}_I + \dot{P}_I - \dot{R}_{VI} - \dot{S}_I \quad (5d)$$

where $\dot{\xi}_i$ (i = η, X, V, I) is the thermal induced fluctuation, $\dot{P}_i$ (i = X, V, I) is the species production rate, $\dot{R}_{VI}$ is the recombination rate, $\dot{S}_i$ (i = V, I) is the source/sink term. The production rate of species $\dot{P}_i = \gamma_i Ran$, where γ_i is related to the *dpa* rate, and *Ran* is the random

number uniformly between 0 and 1. $\dot{R}_{VI} = \nu_r c_V c_I$, where ν_r the recombination rate of vacancy and SIA. To account the faster recombination rate at the void surface, we define it as $\nu_r = \nu_b + \eta^2 \nu_s$. The nucleation/annihilation of vacancy and SIA at the dislocations or grain boundaries are neglected in this paper for simplicity, thus $\dot{S}_V$ and $\dot{S}_I$ are set as zero.

In the simulations, a model size of 89.6 nm × 89.6 nm was used. The time step used for the numerical integration is $t = 0.05$, and the grid spacing is $\Delta l = 0.35$ nm. The model was implemented in a 2D simulation code. Periodic boundary conditions were imposed on the simulation domain. Simi-implicit FFTW method were employed to solve the coupled equations (5a-d) [17].

3. Results and discussion

3.1 Material properties of U-Mo alloy by first-principles calculations

To study the mechanical stability of U-Mo alloys, we investigated the elastic properties of the γ U-Mo alloy phases. Single-crystal elastic constants of a solid phase can be calculated by the stress-strain method [22]. From the predicted elastic constants, the polycrystalline properties including bulk modulus (*B*), shear modulus (*G*), Young's modulus (*E*) and Poisson's ration (*v*) can be determined according to the Voight-Reuss-Hill approach [23], as listed in Table I. For the bcc γ U-Mo alloy phases, the SQS approach will result in elastic tensors with 21 nonvanishing elements. Theoretically, there should be only three independent elastic constants, i.e., C_{11}, C_{12} and C_{44}, for cubic systems. According to Tasnadi et al [24], the closest cubic elastic constants could be obtained via simple averaging,

$$\bar{C}_{11} = \frac{C_{11}+C_{22}+C_{33}}{3}, \bar{C}_{12} = \frac{C_{12}+C_{13}+C_{23}}{3}, and\ \bar{C}_{44} = \frac{C_{44}+C_{55}+C_{66}}{3}. \qquad (6)$$

Upon alloying Mo in γ-U, the shear constant *C*' of γ U-7Mo alloy becomes positive, indicating that the isotropic γ phase of U can be mechanically stabilized by alloying Mo.

Table I. Calculated elastic properties of γ-U and γ U-7Mo, including elastic constants C_{ij} (GPa), shear constant (GPa), bulk modulus (GPa), shear modulus (GPa), Young's modulus (GPa) and Poisson ratio.

	C_{11}	C_{12}	C_{44}	C'	B	G	E	v	Reference
Bcc Mo	466	157	103	155	260	122	316	0.298	This work
	464	158	109	153	260	125	323	0.293	Expt. [25]
γ-U	94	154	34	-30	134	114	225	0.169	This work
U-7Mo	173	138	50	23	143	36	100	0.383	This work

Grain boundary properties, such as grain boundary energy, are important parameters for modeling of grain growth using phase field method. In this work, we only study two representative STGBs in the bcc γ U-7Mo alloy, i.e., Σ3(111)[110] and Σ5(310)[001] GBs. We define the grain boundary energy (γ_{GB}) as

$$\gamma_{GB} = \frac{E_{GB}-E_{SC}}{2A}, \qquad (7)$$

where E_{GB} and E_{SC} are the total energies of the GB supercell and its corresponding single crystal, respectively.

To construct the GBs for the U-Mo alloy phase, the SQS models were applied to the GBs created for bcc metals. Figure 5 shows the created Σ3(111)[110] and Σ5(310)[001] GBs for γ U-

7Mo. The predicted grain boundary energies in the γ U-7Mo alloy are predicted to be 0.37 J/m^2 and 0.63 J/m^2, for Σ3(111)[110] and Σ5(310)[001] GBs, respectively. The grain boundary energies in the U-Mo alloy lie between those of pure γ U and bcc Mo, which is consistent with the predicted elastic properties of these systems.

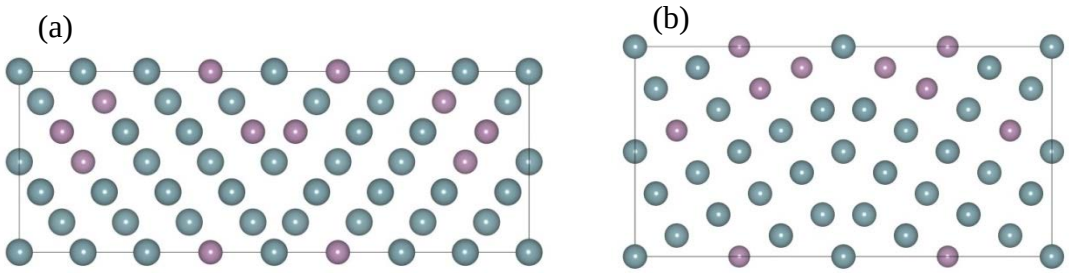

Figure 1. Atomic structures of (a) Σ3(111)[110] and (b) Σ5(310)[001] STGBs for γ U-7Mo alloy. Blue and purple atoms represent the U and Mo atoms, respectively.

3.2 Grain growth by phase field model

To understand statistically averaged kinetics and topological features of heat treated U-Mo alloy, the temporal evolutions of grain structures at different temperatures and with different initial sized grains are studied using an ideal two-dimensional grain growth model by the phase field method. Figure 2 shows the temporal evolution of the grain structure with the initial grain size of ~3 μm annealed at 1000 ^{o}C. Due to the high treating temperature, the grain boundaries move and the grains continue to grow.

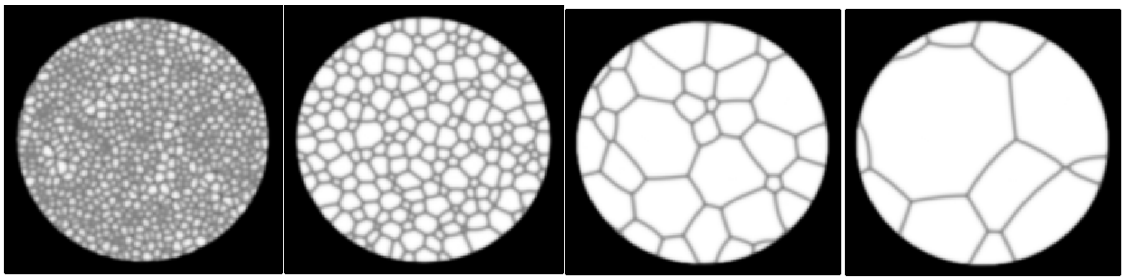

(a) 0 h; (b) 0.083 h; (c) 0.83 h; (d) 3.33 h.

Figure 2. Temporal evolution of the grain structures in U-Mo particle at 1000 ^{o}C: (a) 0 h; (b) 0.083 h; (c) 0.83 h; and (d) 3.33 h.

The time dependence of the averaged grain size in the fuel particle heated at 1000 ^{o}C and 900 ^{o}C are shown in Fig. 3, together with the results from experimentally predicted correlation. A good agreement between our simulations and experimental estimation is obtained for lower temperature case. For higher temperature, the agreement is retained only up to 2 hours of heat treatment. Beyond 2 hours a notable derivation can be observed between these two. This can be explained by the fact that the small number of grains in the fuel particle at the late stage of annealing lead to the large uncertainty of the estimated grain size. Therefore, the initial grain structure has a significant impact on the final grain size. Compared to the U-7Mo grain structures treated at 900 ^{o}C, the averaged grain size is notably larger when heated at 1000 ^{o}C. For example, the average grain size increases from 18 μm to 43 μm after 2 hours when the treating temperature increased from 900 ^{o}C to 1000 ^{o}C. Therefore, the annealing time required for the

desired grain size can be significantly reduced at higher temperatures.

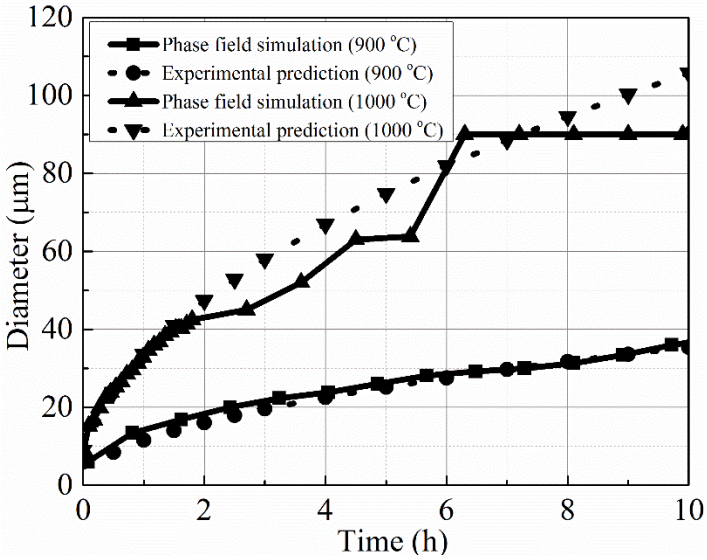

Figure 3. The time dependences of the averaged grain size in U-Mo particles annealed at 900 °C and 1000 °C, respectively, together with the estimated grain size from experiments.

Meanwhile, we also studied the effect of different initial grain structures on the grain growth kinetics [11]. The system with initial 50% 3μm and 50% 15μm (case I) sized grains and 75% 3μm and 25% 15μm (case II) sized grains are taken as two examples. The results show that the grains in Case I evolve notably faster than the one with 100% 3μm sized grains. The reason can be attributed to that a certain amount of large sized grains in the system can help the small sized grain grow faster in the early stage, which makes the averaged grain size increase faster than the pure 3μm case. However, when the system has 75% 3μm and 25% 15μm initial sized grains it evolves even faster than the case with 50% 3μm and 50% 15μm initial sized grains. This result indicates that only a certain small amount of larger size of initial grains can increase the grain growth rate. Therefore, the different initial grain size distribution also plays an important role in the grain growth rate. By using a small amount of larger grain size, the growth rate can be enhanced. Although the mixed initial different size of grains in U-7Mo materials seems unrealistic, the local heat treatment of the particle to locally increase the grain size may be one of the ways to prepare such a sample.

3.3 Fission gas bubble evolution by phase field model

At constant temperature, the formation of gas bubble is driven by the supersaturation of point defects under irradiation. The production and annihilation of defects, especially vacancies, can promote the nucleation and growth of gas bubbles.. Small high-pressurized bubbles are able to grow in size by absorbing both thermal and radiation-induced vacancies. To simulate the gas bubble nucleation and growth in U-Mo, the following parameters are used: production rate of Xe is $\gamma_X = 2.0 \times 10^{-6}$ dpa/s, and SIA is $\gamma_I = 5.0 \times 10^{-6}$ dpa/s, and vacancy is $\gamma_V = 15.0 \times 10^{-6}$ dpa/s. These defect production rates were kept as constants unless the new values are mentioned. Although SIA and vacancy are equally generated during irradiation as Frenkel pairs, SIA often have higher sink rate than vacancy in metals.[26] Therefore biased generation rate for SIA and

vacancy are used in the simulations.

The calculated phase parameter, gas atom, vacancy, and SIA concentrations are plotted as a function of evolution time in Fig. 4, which clearly shows the nucleation and growth processes of gas bubbles under radiation. The Xe bubbles continuously grow under the irradiation. The size of Xe gas bubbles is around 1-3 nm and with the space between them around 10 nm. The gas bubbles appear to be randomly distributed in irradiated U-7Mo. The bubble migration is not considered in this work due to the low mobility of Xe gas bubbles. Therefore, the coalescence only happens when adjacent bubbles grow to contact with each other. Bubble growth is driven by the absorption of vacancies to a void, which must be more probable than the absorption of interstitials to the void. Thus, if a void grows by the absorption of vacancies, more free volume is available for fission gas accumulation inside the void. SIA has lower concentration inside the gas bubble compared with the one in the matrix. The gas bubble pressure largely depends on the ratio of Xe atoms and vacancies inside the bubble.

(a)

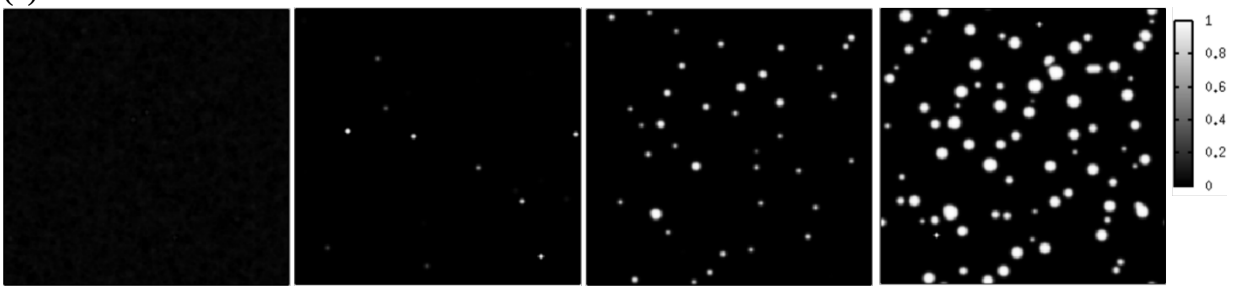

(b)

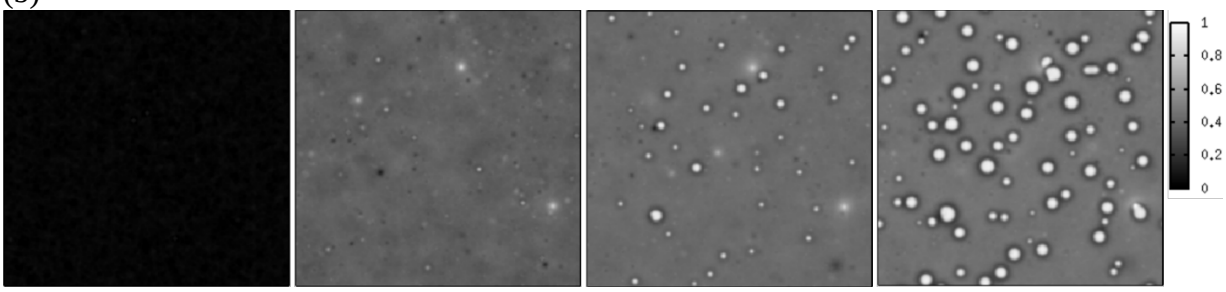

(c)

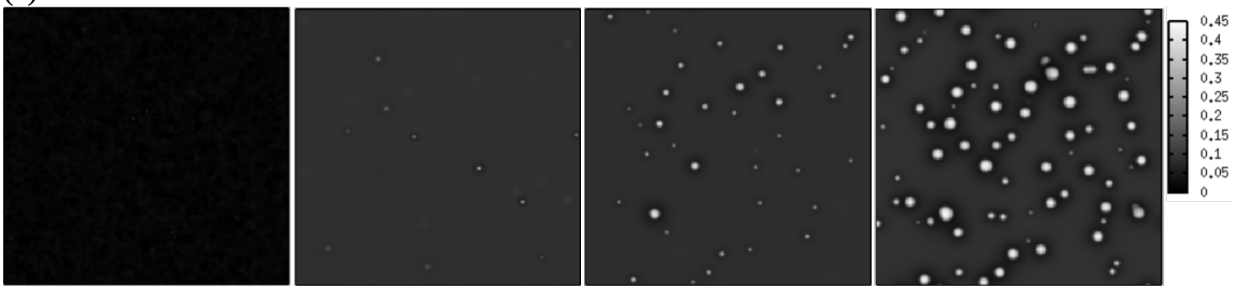

(d)

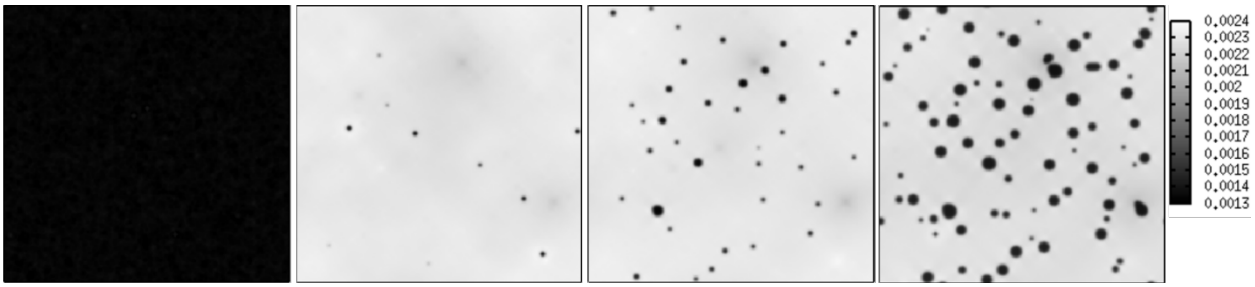

t = 0 h t = 0.056 h t = 0.063 h t = 0.068 h

Figure 4. The temporal evolutions of, (a) phase parameter; (b) vacancy; (c) Xe; (d) SIA in the irradiated U-7Mo single crystal.

The predicted size distribution of gas bubbles is given by Fig. 5. The average size of the gas bubble is about 3.2 nm, which is the classic size of gas bubble in the grains and consistent with the experimental observations [27, 28]. The calculated bubble density is 1.03×10^{16} m^{-2}.

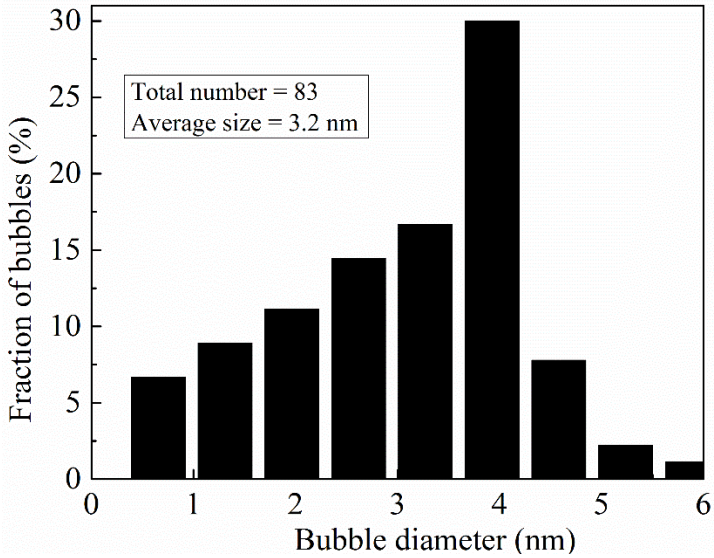

Figure 5. Gas bubble size distribution simulated by the phase field method.

With bubbles residing in the fuel, the fuel swelling can be estimated by a simple relation,

$$\frac{\Delta V}{V} = \frac{V_{AI} - V}{V} \qquad (8)$$

where V is the fabricated volume of fuel, and V_{AI} is the fuel volume together with the gas bubble volume. The effect of vacancy production rate on the swelling and the gas bubble size distribution are computed and shown in Fig. 6. With higher irradiation rate, the beginning time of swelling is obviously earlier and swelling of fuel is also larger, which agrees with the experimental observations.[27] The measured bubble size distribution shows that the higher irradiation rate the larger average bubble size is. And also the distribution of bubble size is broader as with higher irradiation rate. This is consistent with the recent experimental results performed in a pure Mo fuel [27]. The averaged bubble size increases from 3.2 nm to 4.0 nm

when the vacancy production rate of vacancy increases from 15.0×10^{-6} dpa/s to 17.0×10^{-6}dpa/s. These results show that fuel swelling is very sensitive to the fission rate.

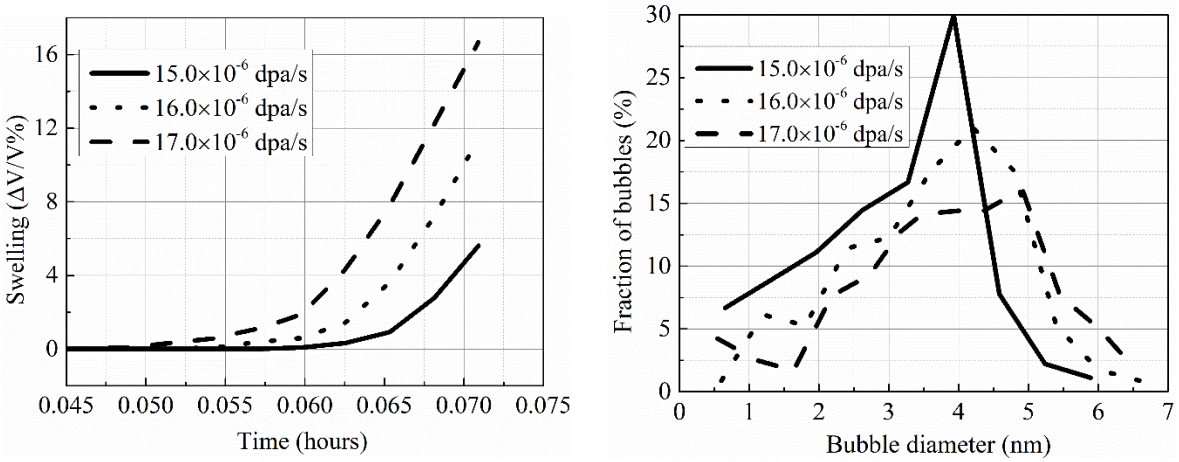

(a) (b)

Figure 6. The effect of vacancy production rate on the fuel swelling (a), and the bubble size distribution (b).

The different sink strength for vacancy and SIA can result in biased production rates of vacancy and SIA in U-Mo. We also study three different production rates of SIA to illustrate its effect on the fuel swelling and the bubble size distribution.[21] Our calculated results show that increased SIA production rate can lead to reduced fuel swelling. This can be explained by the fact that higher SIA concentration can result in faster recombination of vacancy and SIA during the irradiation, thus reduced vacancy concentration. This suggests that artificially reducing the sink strength of SIA can help to decrease the size of gas bubbles and therefore fuel swelling.

4. Conclusions

The U-Mo fuel system was studied by using a multiscale simulation approach. DFT calculations were used to study the stability of bcc U-Mo alloys based on the enthalpy of formation and elastic properties. Two grain boundaries, i.e., Σ3(111)[110] and Σ5(310)[001], were investigated for γ U-7Mo and compared with those of pure bcc Mo and U metals. Using the predicted grain boundary properties as input parameters, we studied the effects of annealing temperature, annealing time and initial grain structure on the grain growth in U-7Mo alloy particles by the phase field approach. Increasing temperature of heat treatment is found to the most efficient way to reduce the annealing time for desired grain size.

The gas bubble evolution was investigated in irradiated U-7Mo. The calculated bubble size distribution and fuel swelling are consistent with the experimental observations. The increased production rate of vacancies leads to increased bubble size and fuel swelling, and the opposite is true for SIA. These results provide a foundation for the future study of intergranular gas bubble kinetics in U-Mo. We expect the currently predicted kinetic model for the grain growth in the U-7Mo will be helpful in determining the optimal experimental conditions.

5. Acknowledgement

This work is sponsored by the U.S. Department of Energy, National Nuclear Safety

Administration (NNSA), Office of Material Management and Minimization (NA-23) Reactor Conversion Program.

6. References

[1] P.E. Blöchl, Physical Review B 50 (1994) 17953.
[2] G. Kresse, J. Furthmüller, Phys. Rev. B 54 (1996) 11169.
[3] G. Kresse, D. Joubert, Phys. Rev. B 59 (1999) 1758.
[4] J.P. Perdew, K. Burke, M. Ernzerhof, Phys. Rev. Lett. 77 (1996) 3865.
[5] A. van de Walle, G. Ceder, Journal of Phase Equilibria 23 (2002) 348.
[6] A. van de Walle, P. Tiwary, M. de Jong, D.L. Olmsted, M. Asta, A. Dick, D. Shin, Y. Wang, L.Q. Chen, Z.K. Liu, Calphad 42 (2013) 13.
[7] H. Ogawa, MATERIALS TRANSACTIONS 47 (2006) 2706.
[8] Z.-G. Mei. unpublished work.
[9] D. Fan, L.Q. Chen, Acta Materialia 45 (1997) 611.
[10] D.N. Fan, C.W. Geng, L.Q. Chen, Acta Materialia 45 (1997) 1115.
[11] Z.-G. Mei, L. Liang, Y.S. Kim, W. Tom, E.O. Hare, A.M. Yacout, G. Hofman, M. Anitescu, Journal of Nuclear Materials (2015).
[12] I. Steinbach, Annual Review of Materials Research, Vol 43 43 (2013) 89.
[13] M. Wang, B.Y. Zong, G. Wang, Computational Materials Science 45 (2009) 217.
[14] N. Moelans, B. Blanpain, P. Wollants, Physical Review B 78 (2008).
[15] D.C. Blaine, J.D. Gurosik, S.J. Park, D.F. Heaney, R.M. German, Metallurgical and Materials Transactions a-Physical Metallurgy and Materials Science 37A (2006) 715.
[16] D.E. Smirnova, A.Y. Kuksin, S.V. Starikov, Journal of Nuclear Materials 458 (2015) 304.
[17] L.Q. Chen, J. Shen, Computer Physics Communications 108 (1998) 147.
[18] L.Q. Chen, Annual Review of Materials Research 32 (2002) 113.
[19] P.C. Millett, A. El-Azab, S. Rokkam, M. Tonks, D. Wolf, Computational Materials Science 50 (2011) 949.
[20] P.C. Millett, A. El-Azab, D. Wolf, Computational Materials Science 50 (2011) 960.
[21] L. Liang, Z.-G. Mei, Y.S. Kim, T. Wiencek, G. Hofman, M. Anitescu, A.M. Yacout. Intragranular Gas bubble kinetics in an irradiated U-Mo fuel using a multistate simulation approach. 2015.
[22] S. Shang, Y. Wang, Z.-K. Liu, Applied Physics Letters 90 (2007) 101909.
[23] D.H. Chung, W.R. Buessem, Journal of Applied Physics 38 (1967) 2535.
[24] F. Tasnádi, M. Odén, I.A. Abrikosov, Physical Review B 85 (2012) 144112.
[25] J.M. Dickinson, P.E. Armstrong, Journal of Applied Physics 38 (1967) 602.
[26] L. Pagano, A.T. Motta, R.C. Birtcher, Journal of Nuclear Materials 244 (1997) 295.
[27] D. Yun, M.A. Kirk, P.M. Baldo, J. Rest, A.M. Yacout, Z.Z. Insepov, Journal of Nuclear Materials 437 (2013) 240.
[28] B.D. Miller. Microstructural studies of uranium-7wt%molybdenum/aluminum-2wt%silicon dispersion fuel. University of wisconsin-madison, 2010.